

## Optical investigation of $\text{Eu}^{3+}$ in a sodium borosilicate glass: Evidence for two different site distributions

G. Pucker, K. Gatterer, and H. P. Fritzer

*Institut für Physikalische und Theoretische Chemie, Graz University of Technology, A-8010 Graz, Austria*

M. Bettinelli

*Sezione di Chimica, Istituto Policattedra, Facoltà di Scienze Matematiche, Fisiche e Naturali, Università di Verona, I-37134 Verona, Italy*

M. Ferrari

*Consiglio Nazionale delle Ricerche CeFSA Centro Fisica Stati Aggregati, I-38050 Povo, Trento, Italy*

(Received 5 September 1995; revised manuscript received 4 December 1995)

A borosilicate glass of molar composition  $0.01\text{Eu}_2\text{O}_3 \cdot 0.99(25\text{Na}_2\text{O} \cdot 50\text{B}_2\text{O}_3 \cdot 25\text{SiO}_2)$  has been studied through the optical spectroscopy of the  $\text{Eu}^{3+}$  ion. Absorption and excitation spectra, fluorescence line narrowing, and time-resolved spectroscopy show that the impurity ions are accommodated in two different site distributions, one related to a silicate environment, and the other one related to a borate environment. These results have been corroborated by crystal-field calculations and comparison with the crystal-field parameters for the  $\text{Eu}^{3+}$  ion in silicate and borate glasses. The presence of phonon sidebands indicates strong coupling with high-frequency Si-O and B-O stretching vibrational modes.

### I. INTRODUCTION

Borosilicate glasses have found many technological applications ranging among others, from shock resistant laboratory glasses, to optical glasses and to dumps for nuclear waste materials.<sup>1,2</sup> The properties of the glasses depend on their internal structure, which is governed by competitive network formation of the various borate and silicate structural groupings. For ternary sodium borosilicate glasses two compositional parameters  $R = \text{Na}_2\text{O}/\text{B}_2\text{O}_3$  and  $K = \text{SiO}_2/\text{B}_2\text{O}_3$  are useful to describe the network modification as a function of composition. The most detailed information about the structure comes from wide-line  $^{11}\text{B}$  NMR data. For  $R < 0.5$ , a model developed by Bray and co-workers,<sup>3-5</sup> suggests that in this low sodium content range all boron is either coordinated by three oxygens (trigonal  $\text{BO}_3$  units) or by four oxygens (tetrahedral  $\text{BO}_4^-$  units). The sodium charges compensate tetrahedral boron sites. The maximum sodium content, which can be accommodated in the borate phase, is assumed to correspond to the diborate composition, which is reached at  $R = 0.5$ . In this regime the sodium borate and silicate portions of the glass do not mix. This aspect is supported by the tendency of these glasses to phase separation. However, Raman and recent NMR investigations<sup>6,7</sup> indicate that small amounts of sodium are also incorporated in the silicate network starting at about  $R = 0.30$ , leading to the formation of nonbridging oxygens in the silicate portion of the glass. This behavior is also confirmed by measurements of the phonon sidebands of  $\text{Eu}^{3+}$ -doped sodium borosilicate glasses in this compositional range.<sup>8</sup>

At  $R \geq 0.5$ , according to Bray *et al.*, the excess of sodium enters the silicate network under formation of nonbridging oxygens and, at the same time,  $\text{BO}_4^-$  units are incorporated into the silicate network. These two species are accommodated on different network sites.<sup>7</sup>

The composition of the sample used for the present investigation has  $R = 0.5$  and  $K = 0.5$  and therefore lies at the border of the two regimes. It is interesting to confirm the model outlined above using laser-excited optical spectroscopy of the probe ion  $\text{Eu}^{3+}$ .

Laser-excited site-selective spectroscopy, commonly called fluorescence-line narrowing (FLN), has been demonstrated to be an extremely useful technique for the study of structural inhomogeneities in glasses.<sup>9-11</sup> The majority of investigations has been carried out with  $\text{Eu}^{3+}$  as a structural probe because of its unique energy level structure<sup>12-21</sup> and the singlet to singlet nature of the  $^5D_0 \rightarrow ^7F_0$  transition. While most of the FLN investigations have been performed on  $\text{Eu}^{3+}$  ions in single phase media the usefulness of this technique for multiphase materials and glass ceramics has also been shown.<sup>22-27</sup>

In the present investigation the FLN signal was recorded nonresonantly with the laser beam. The observed changes of the emission spectra as a function of the excitation wavelength are discussed in terms of the local environment of the  $\text{Eu}^{3+}$  ions in the sample, using elementary crystal-field theory. Further information on the energy-level structure of  $\text{Eu}^{3+}$  in the host glass was obtained by FLN after excitation into the  $^5D_1$  state. The results of the FLN experiments were complemented by excitation spectra in the  $^7F_0 \rightarrow ^5D_0$  and the  $F_0 \rightarrow ^5D_1$  regions including the phonon sideband structure of the  $^5D_0 \rightarrow ^7F_0$  transition. To the best of our knowledge the present investigation is the only work on FLN in  $\text{Eu}^{3+}$  doped sodium borosilicate glasses with the exception of an older work by Alimov *et al.*<sup>13</sup> in which energy migration as a function of the  $\text{Eu}^{3+}$  concentration is discussed.

### II. EXPERIMENTAL

Glasses with the molar composition  $0.01\text{Eu}_2\text{O}_3 \cdot 0.99(25\text{Na}_2\text{O} \cdot 50\text{B}_2\text{O}_3 \cdot 25\text{SiO}_2)$  were prepared by

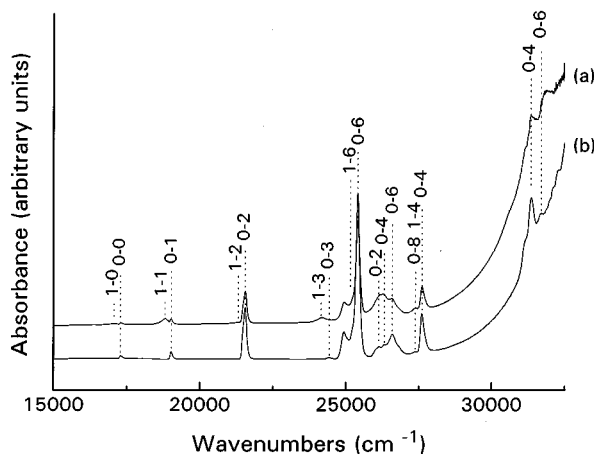


FIG. 1. Absorption spectra of  $\text{Eu}^{3+}$  in the  $25\text{Na}_2\text{O}\cdot 50\text{B}_2\text{O}_3\cdot 25\text{SiO}_2$  glass recorded at 300 K (a) and at 20 K (b). Transitions  ${}^7F_J \rightarrow {}^{2S+1}L_{J'}$  are labeled by  $J-J'$ .

melting appropriate amounts of analytical grade  $\text{H}_3\text{BO}_3$ ,  $\text{Na}_2\text{CO}_3$ ,  $\text{SiO}_2$ , and  $\text{Eu}_2\text{O}_3$  (99.999%) at 1350 °C in platinum crucibles under air. Samples were obtained by quenching the melt on steel plates or by pouring the melt into a graphite mould. For the optical measurements the sample surfaces were ground and polished.

The composition given above corresponds to the batch composition. Possible small changes caused by vaporization during melting are neglected. All experiments were carried out on quenched samples without annealing in order to make comparisons possible with NMR measurements, which are usually performed on quenched samples.<sup>3,5</sup>

Absorption spectra in the visible range were obtained using a double monochromator absorption spectrophotometer with  $f=0.25$  m. 100 spectra of the sample were accumulated and in this way the weak features in the  $\text{Eu}^{3+}$  absorption spectra could be accurately obtained. Low-resolution luminescence spectra in the UV-VIS region were measured at room temperature using a spectrofluorimeter with spectral bandwidths of 1.5 nm.

A dye laser pumped by an excimer laser was used to collect high-resolution emission and excitation spectra. The laser had a typical linewidth of  $0.3\text{ cm}^{-1}$  full width at half maximum (FWHM). The luminescence signal was monitored with a double monochromator in the photon counting mode. The time-resolved signal was measured at different delay times with respect to the excitation pulse and with different temporal windows.

Emission decays were measured with a multichannel analyser with a dwell time of  $5.12\ \mu\text{s}$ . Low-temperature measurements were carried out at 13–20 K using helium cryostats.

### III. RESULTS

#### A. Absorption spectra

The absorption spectra of  $\text{Eu}^{3+}$  in the  $0.25\text{Na}_2\text{O}\cdot 0.50\text{B}_2\text{O}_3\cdot 0.25\text{SiO}_2$  glass recorded at 300 and 20 K are shown in Figs. 1(a) and 1(b). Because of the close proximity of both the  ${}^7F_1$  (about  $200\text{ cm}^{-1}$ ) and  ${}^7F_2$  (about  $1000\text{ cm}^{-1}$ ) states to the ground state  ${}^7F_0$ , the room-

TABLE I. Russell-Saunders assignments of the optical transitions in the absorption spectrum of  $\text{Eu}^{3+}$  in the  $25\text{Na}_2\text{O}\cdot 50\text{B}_2\text{O}_3\cdot 25\text{SiO}_2$  glass, positions of the barycenters in wave numbers and oscillator strengths of some transitions. Oscillator strengths labeled with  $a$ ,  $b$ , and  $c$  were used for evaluating  $\Omega_2$ ,  $\Omega_4$ , and  $\Omega_6$ , respectively.

$J-J'$ in Fig. 1	${}^{2S+1}L_J$ assignment	Barycenter ( $\text{cm}^{-1}$ )	Oscillator strength
	${}^7F_2 \rightarrow {}^5D_0$	16 352	
1-0	${}^7F_1 \rightarrow {}^5D_0$	16 913	
0-0	${}^7F_0 \rightarrow {}^5D_0$	17 288	
	${}^7F_2 \rightarrow {}^5D_1$	18 094	
1-1	${}^7F_1 \rightarrow {}^5D_1$	18 656	$3.0 \times 10^{-7} a$
0-1	${}^7F_0 \rightarrow {}^5D_1$	19 007	
	${}^7F_2 \rightarrow {}^5D_2$	20 567	
1-2	${}^7F_1 \rightarrow {}^5D_2$	21 190	
0-2	${}^7F_0 \rightarrow {}^5D_2$	21 539	$3.4 \times 10^{-7} a$
	${}^7F_2 \rightarrow {}^5D_3$	23 435	
1-3	${}^7F_1 \rightarrow {}^5D_3$	24 163	
0-3	${}^7F_0 \rightarrow {}^5D_3$	24 417	
1-6	${}^7F_1 \rightarrow {}^5L_6$	25 050	
0-6	${}^7F_0 \rightarrow {}^5L_6$	25 401	$15.5 \times 10^{-7} c$
0-2	${}^7F_0 \rightarrow {}^5G_2$	26 132	
0-4	${}^7F_0 \rightarrow {}^5G_4$	26 337	
0-6	${}^7F_0 \rightarrow {}^5G_6$	26 581	
0-8	${}^7F_0 \rightarrow {}^5L_8$	27 380	
1-4	${}^7F_1 \rightarrow {}^5D_4$	27 380	
0-4	${}^7F_0 \rightarrow {}^5D_4$	27 594	$2.6 \times 10^{-7} b$
0-4	${}^7F_0 \rightarrow {}^5H_4$	31 353	
0-6	${}^7F_0 \rightarrow {}^5H_6$	31 662	

temperature spectrum contains also transitions starting from these excited states. The corresponding “hot bands” are absent in the low-temperature spectrum. The individual transitions are labeled by  $J-J'$ , the  $J$  values of the initial  ${}^7F_J$  and the final  ${}^{2S+1}L_{J'}$  state. Transitions starting from  ${}^7F_2$  are too weak to be seen on the condensed scale of Fig. 1(a). The  ${}^7F_0 \rightarrow {}^5D_0$  transition of  $\text{Eu}^{3+}$  is forbidden by electric dipole and magnetic dipole mechanisms. Consequently, it constitutes one of the weakest features in the spectrum. Its intensity is about three times smaller than the intensity of the  ${}^7F_0 \rightarrow {}^5D_1$  transition which is magnetic dipole allowed. The  ${}^7F_0 \rightarrow {}^5D_0$  absorption band at 20 K has a maximum at  $17\,288\text{ cm}^{-1}$  and an inhomogeneous width of  $110\text{ cm}^{-1}$ , to compare with the width range  $92\text{--}111\text{ cm}^{-1}$  for the same transition in sodium borate glasses and  $69\text{--}96\text{ cm}^{-1}$  in sodium silicate glasses.<sup>28</sup>

The Russell-Saunders assignments and the band positions are given in Table I together with the oscillator strengths for those transitions which were used for a Judd-Ofelt analysis. The Judd-Ofelt intensity parameters  $\Omega_\lambda$  ( $\lambda=2,4,6$ ) were obtained in the usual way<sup>19</sup> from the room-temperature absorption spectrum and are found to be  $\Omega_2=12.9 \times 10^{-20}\text{ cm}^2$ ,  $\Omega_4=5.9 \times 10^{-20}\text{ cm}^2$ , and  $\Omega_6=2.7 \times 10^{-20}\text{ cm}^2$ . It is well known, that intensity parameters calculated from the oscillator strengths of  $\text{Eu}^{3+}$  containing samples are not very reliable. However, the present Judd-Ofelt parameters are in the range commonly observed for oxide glasses.<sup>19,29–32</sup>

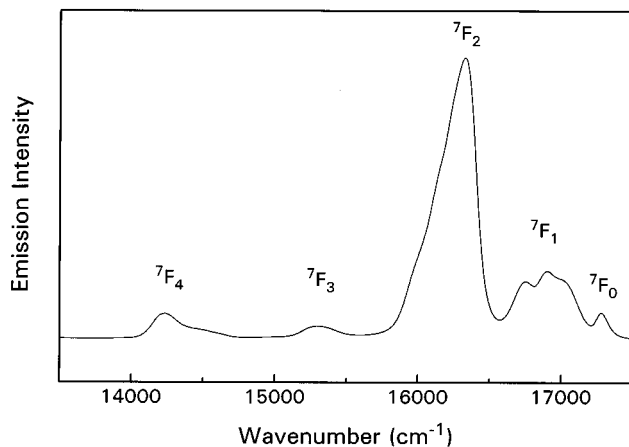


FIG. 2. Room-temperature low-resolution luminescence spectrum of  $\text{Eu}^{3+}$  in the  $25\text{Na}_2\text{O}\cdot 50\text{B}_2\text{O}_3\cdot 25\text{SiO}_2$  glass in the  ${}^5D_0 \rightarrow {}^7F_J$  ( $J=0-4$ ) region obtained after broadband excitation at 394 nm.

### B. Non-site-selective emission

The room-temperature low-resolution luminescence spectrum of the glass in the  $13\,500\text{--}17\,500\text{ cm}^{-1}$  range obtained after broadband excitation at 394 nm in the  ${}^5L_6$  state is shown in Fig. 2. Only emission from the  ${}^5D_0$  to the final  ${}^7F_J$  ( $J=0-4$ ) states is observed. The electric and magnetic dipole forbidden  ${}^5D_0 \rightarrow {}^7F_0$  transition is centered at  $17\,290\text{ cm}^{-1}$  and has a FWHM of approximately  $120\text{ cm}^{-1}$ . The magnetic dipole transition  ${}^5D_0 \rightarrow {}^7F_1$  is present in the region  $17\,200\text{--}16\,560\text{ cm}^{-1}$ . The Stark splitting is not well resolved. The lowest energy Stark component is situated at  $16\,750\text{ cm}^{-1}$ , while the other components strongly overlap. The most intense emission is centered at  $16\,314\text{ cm}^{-1}$  and corresponds to the  ${}^5D_0 \rightarrow {}^7F_2$  electric dipole transition. The band is completely unresolved with a FWHM of about  $300\text{ cm}^{-1}$ . The weak and broad transitions centered at about  $15\,300$  and  $14\,360\text{ cm}^{-1}$  correspond to the transitions  ${}^5D_0 \rightarrow {}^7F_3$  and  ${}^5D_0 \rightarrow {}^7F_4$ , respectively.

The ratio of the intensities of the  ${}^5D_0 \rightarrow {}^7F_2$  and the  ${}^5D_0 \rightarrow {}^7F_1$  transitions gives a measure of the degree of distortion from inversion symmetry of the local environment of the  $\text{Eu}^{3+}$  ion in glasses. In fact, the  ${}^5D_0 \rightarrow {}^7F_1$  transition is magnetic dipole allowed and its strength is not strongly site dependent, whilst the  ${}^5D_0 \rightarrow {}^7F_2$  transition is forbidden and becomes electric dipole allowed in odd field. The present value of 3.3 lies well within the range of values usually found in oxide glasses, indicating that the  $\text{Eu}^{3+}$  ions occupy low-symmetry sites.<sup>33</sup> The position and FWHM of the  ${}^5D_0 \rightarrow {}^7F_0$  transition is unchanged compared with the absorption spectrum, which indicates that energy-transfer processes involving  $\text{Eu}^{3+}$  ions are not important in the glass under investigation.

### C. Emission after selective ${}^5D_0$ excitation

Emission was obtained after excitation at different energies inside the absorption profile of the  ${}^7F_0 \rightarrow {}^5D_0$  transition. The  ${}^5D_0 \rightarrow {}^7F_1$  transition is clearly structured due to the Stark splitting of the terminal state, whereas the  ${}^5D_0 \rightarrow {}^7F_2$  transition is not well resolved. Brecher and Riseberg<sup>12</sup> in their classical paper on FLN of  $\text{Eu}^{3+}$  in a sodium barium zinc silicate glass were able to fit five components into the observed  ${}^5D_0 \rightarrow {}^7F_2$  profile. We did not adopt this procedure for our glass. It will become evident from the discussion of the  ${}^5D_0 \rightarrow {}^7F_1$  transition that the  $\text{Eu}^{3+}$  ions are located in two major types of sites each having a  ${}^7F_1$  state split into three components. The  ${}^7F_2$  state will be split into five components in each site distribution and, therefore, the observed  ${}^5D_0 \rightarrow {}^7F_2$  profile is a convolution of at least ten transitions between Stark levels, which makes any fitting procedure quite unreliable. For the following discussion only the transitions to the  ${}^7F_1$  Stark levels are considered.

Figure 3 shows the time-resolved site-selective emission spectra of the  ${}^5D_0 \rightarrow {}^7F_1$  transition at 13 K as a function of the excitation energy which is indicated at the right side of each trace. All spectra reproduced in the figures were collected with a delay of  $50\text{ }\mu\text{s}$  delay and an acquisition time of 5 ms after the laser pulse.

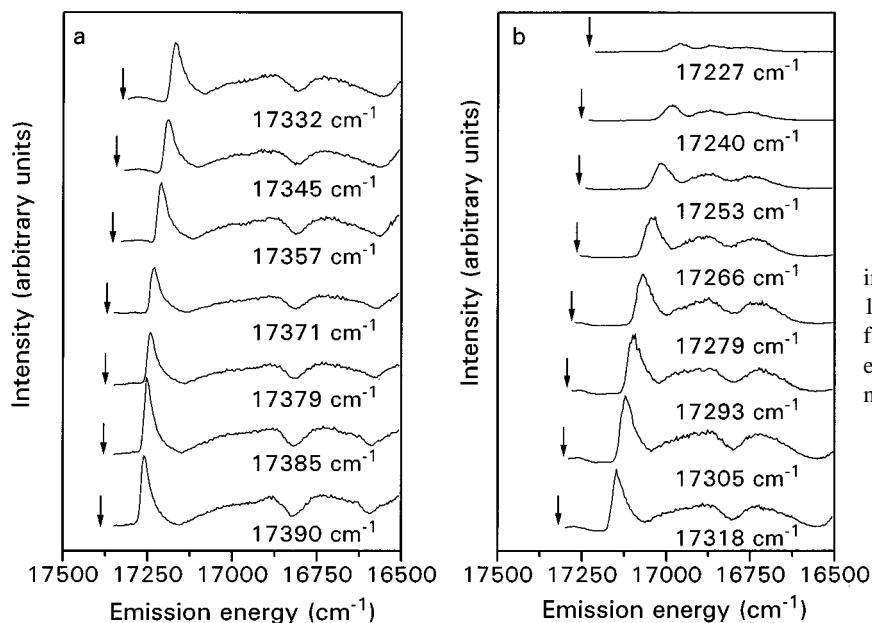


FIG. 3.  ${}^5D_0 \rightarrow {}^7F_1$  emission spectra of  $\text{Eu}^{3+}$  in the  $25\text{Na}_2\text{O}\cdot 50\text{B}_2\text{O}_3\cdot 25\text{SiO}_2$  glass recorded at 13 K with a  $50\text{ }\mu\text{s}$  delay and 5 ms gate as a function of the excitation energy. The excitation energy is indicated by the arrow and the wave number.

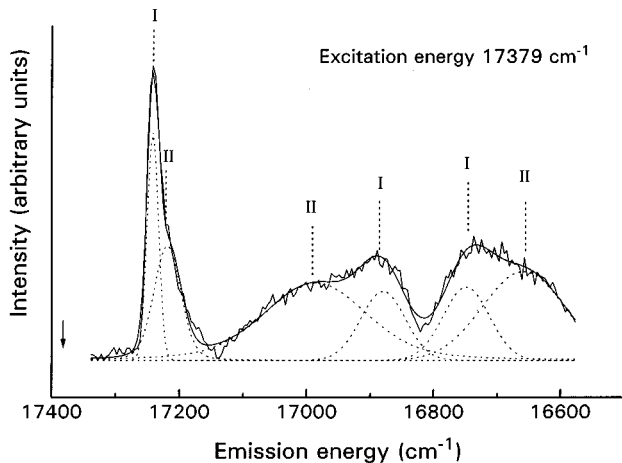


FIG. 4. Fit of six Voigt-profile components to the emission spectrum of  $\text{Eu}^{3+}$  in the  $25\text{Na}_2\text{O}\cdot 50\text{B}_2\text{O}_3\cdot 25\text{SiO}_2$  glass recorded at 13 K after  $17\,379\text{ cm}^{-1}$  excitation.

Changes in the positions and shapes of the Stark levels in Fig. 3 are clearly seen. The band corresponding to the transition terminating on the lowest component of the  ${}^7F_1$  state is narrower than the other ones and its position more sensitive to the excitation wavelength. It is evident that for nearly all spectra at least five components can be easily identified. In principle, there are two explanations for the appearance of more than the three lines expected in a FLN experiment for a  ${}^5D_0 \rightarrow {}^7F_1$  transition of  $\text{Eu}^{3+}$ . One is phonon-assisted energy transfer to lower energy sites,<sup>13,18</sup> the other is the existence of  $\text{Eu}^{3+}$  in two different environments<sup>21,22,25</sup> in the glass host. The presence of energy transfer was checked by measuring decay curves of the emitting state and time-resolved spectra. After excitation at  $17\,300\text{ cm}^{-1}$  (inside the  ${}^5D_0 \rightarrow {}^7F_0$  transition) decay curves were recorded at 123 and 18 K monitoring at  $16\,225\text{ cm}^{-1}$  (inside the  ${}^5D_0 \rightarrow {}^7F_2$  transition). The decay curves are nearly single exponential with decay times of 1.84 ms both at 123 and 18 K.

Furthermore, other FLN spectra were recorded with delay times of 30 and 700  $\mu\text{s}$  after the excitation pulse and acquisition times of 1 and 4 ms, respectively. The spectra of the  ${}^5D_0 \rightarrow {}^7F_1$  region recorded with different delay times and different gates were unchanged. Since it is known that especially the lowest  ${}^7F_1$  Stark level is very sensitive to energy transfer,<sup>20</sup> we conclude that this process is negligible at the present  $\text{Eu}^{3+}$  concentration. Both the temperature-independent nearly single exponential decay and the absence of time evolution of the  ${}^5D_0 \rightarrow {}^7F_1$  spectra suggest that the additional spectral features are caused by simultaneous excitation of  $\text{Eu}^{3+}$  ions in two different site distributions.

The emission spectra of the  ${}^5D_0 \rightarrow {}^7F_1$  transition were deconvoluted into six Voigt-type components. A fit is shown in Fig. 4. The positions of the six Stark levels obtained from the deconvolution are plotted in the lower part of the energy-level diagram in Fig. 5 as a function of the excitation energy (the energy of the  ${}^7F_0$  state is taken as zero). It is evident that the  ${}^7F_1$  splitting increases steadily with the  ${}^5D_0 \rightarrow {}^7F_0$  energy. The assignment of the Stark components  $\epsilon_0$ ,  $\epsilon_+$ , and  $\epsilon_-$  to the two major types of sites (I,II) is discussed in Sec. IV.

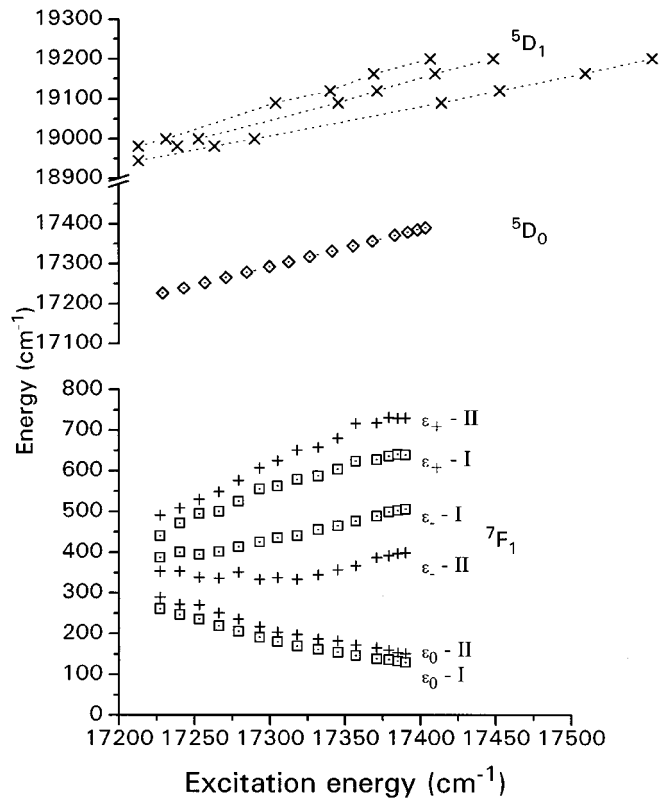


FIG. 5. Plot of the  ${}^7F_1$ ,  ${}^5D_0$ , and  ${}^5D_1$  Stark levels of  $\text{Eu}^{3+}$  in the  $25\text{Na}_2\text{O}\cdot 50\text{B}_2\text{O}_3\cdot 25\text{SiO}_2$  glass at 13 K as a function of the  ${}^7F_0 \rightarrow {}^5D_0$  energy. The  ${}^7F_0$  ground state is taken as the zero of energy. Levels assigned to the silicate and borate environments are labeled by I and II, respectively (see text).

#### D. Emission after ${}^5D_1$ excitation

The  ${}^7F_0 \rightarrow {}^5D_1$  absorption band is centered at  $19\,010\text{ cm}^{-1}$  with a FWHM of about  $95\text{ cm}^{-1}$ . The Stark splitting of the  ${}^5D_1$  state is unresolved. Emission spectra were recorded after excitation at different energies inside the inhomogeneously broadened profile of this band. In Fig. 6 the emission spectra for two different excitation energies are shown. Whilst in Fig. 6(a) the excitation was at low energy, in Fig. 6(b) the high-energy tail of the  ${}^7F_0 \rightarrow {}^5D_1$  absorption profile was excited. The most remarkable difference between Figs. 6(a) and 6(b) is the presence of more than one line in the region of the  ${}^5D_0 \rightarrow {}^7F_0$  transition in the latter. It has been shown by Hegarty, Yen, and Weber<sup>14</sup> in their investigation of  $\text{Eu}^{3+}$ -doped lithium borate glass that this behavior is perfectly consistent with the shift of the centers of gravity and the increasing Stark splitting of the  ${}^5D_1$  multiplet of  $\text{Eu}^{3+}$  in sites of increasing local crystal-field strength. In fact, for excitation energies in the  $19\,000\text{--}19\,200\text{ cm}^{-1}$  range [e.g., Fig. 6(b)] up to three subsets of ions all differing in their detailed  ${}^5D_1$  structure may be excited.<sup>14</sup> In each subset a different Stark level is in resonance with the laser. These subsets of ions being different in their  ${}^5D_1$  states will also have their  ${}^5D_0$  state at a different energy and their  ${}^5D_0 \rightarrow {}^7F_0$  transitions will be consequently displaced.

Excitation into the low-energy part of the  ${}^7F_0 \rightarrow {}^5D_1$  transition [Fig. 6(a)], by which only the lowest Stark component of the  ${}^5D_1$  state is likely to be populated, gives rise only to one  ${}^5D_0 \rightarrow {}^7F_0$  emission line. However, in this case there is

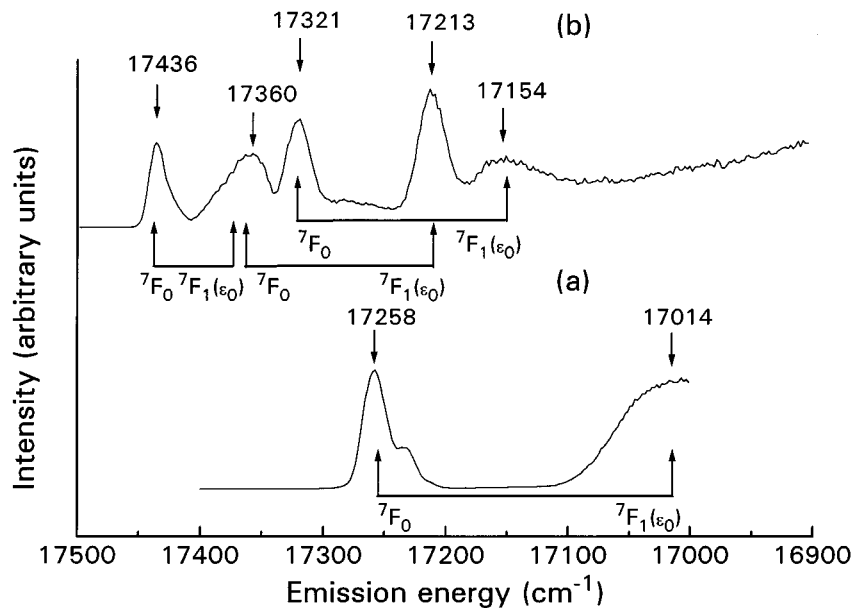


FIG. 6. Emission spectra of  $\text{Eu}^{3+}$  in the  $25\text{Na}_2\text{O}\cdot 50\text{B}_2\text{O}_3\cdot 25\text{SiO}_2$  glass after excitation at  $18\,982\text{ cm}^{-1}$  (a) and  $19\,120\text{ cm}^{-1}$  (b) inside the  ${}^7F_0 \rightarrow {}^5D_1$  band, recorded at 13 K. The maxima of luminescence bands and relative assignment are labeled in order to have an easy comparison with Fig. 5.

also a small probability of exciting the other Stark components of states having the  ${}^5D_1$  barycenter at lower energy, causing the low-energy shoulder. Therefore the emission spectra after  ${}^5D_1$  excitation can be related to the ones obtained after  ${}^5D_0$  excitation, with the advantage that the  ${}^5D_0 \rightarrow {}^7F_0$  transition is also observable. The offsets of the different  ${}^5D_0 \rightarrow {}^7F_0$  transitions reveal the Stark splitting of the  ${}^5D_1$  state. This splitting plotted against the excitation energy is included in the upper part of Fig. 5 and in Fig. 8.

In the present experiment it is not possible to distinguish between the two site distributions evidenced in the the FLN of the  ${}^5D_0 \rightarrow {}^7F_1$  transition. This is attributed to the fact that the splitting of  ${}^5D_1$  is roughly five times smaller than the one of  ${}^7F_1$ , and therefore the relatively small differences in the crystal fields of the borate and of the silicate sites cannot be detected. The asymmetry of the  ${}^5D_0 \rightarrow {}^7F_0$  transitions which is best seen in the isolated  $17\,436\text{ cm}^{-1}$  band in Fig. 6(b) may however be taken as an indication for the existence of  $\text{Eu}^{3+}$  ions in two environments.

The remaining features of the emission spectra can be attributed to transitions from the individual  ${}^5D_0$  states to the corresponding  ${}^7F_1(\epsilon_0)$  levels which are also expected in this spectral region. The positions of these transitions for each  ${}^5D_0$  state energy may be obtained from the energy-level diagram in Fig. 5 and are indicated in Fig. 6 by connecting arrows.

### E. Excitation spectra

Site-selective excitation spectra were obtained by tuning the dye laser over the energy range of the  ${}^7F_0 \rightarrow {}^5D_0$  and  ${}^7F_0 \rightarrow {}^5D_1$  regions. Moreover, from about  $900$  to  $1700\text{ cm}^{-1}$  above the  ${}^7F_0 \rightarrow {}^5D_0$  transition a phonon sideband structure is observed. Since phonon sidebands correspond to localized vibrational modes around  $\text{Eu}^{3+}$ , they contain important information about the surrounding of the structural probes.

#### ${}^5D_1$ region

For excitation spectra in the  ${}^7F_0 \rightarrow {}^5D_1$  region the laser was tuned from  $18\,900$  to  $19\,400\text{ cm}^{-1}$  and emission was

monitored at different positions inside the  ${}^5D_0 \rightarrow {}^7F_0$  band. Figure 7 shows the excitation spectrum for a low observation energy ( $17\,233\text{ cm}^{-1}$ ). The positions of the three bands centered at about  $19\,000\text{ cm}^{-1}$  agree very well with the splitting of a  ${}^5D_1$  state predicted for a  $\text{Eu}^{3+}$  site with a  ${}^5D_0 \rightarrow {}^7F_0$  energy of  $17\,233\text{ cm}^{-1}$  (see Fig. 5). Three additional bands corresponding to  ${}^5D_0 \rightarrow {}^7F_1(\epsilon_0)$  are expected, but only two bands at  $19\,068$  and  $19\,134\text{ cm}^{-1}$  are observed, due to the decreasing excitation intensity of the dye laser in this region. From the energy-level diagram (Fig. 5) the  ${}^5D_0 \rightarrow {}^7F_0$  transition energy for these two bands can be estimated at about  $17\,360\text{ cm}^{-1}$ .

The present  ${}^5D_1$  excitation spectra thus confirm the  ${}^5D_1$  splitting obtained by emission after  ${}^5D_1$  excitation. The agreement of the two experiments is excellent (see Fig. 8). The smaller observation range of the excitation experiment is caused by the rapid decrease of the laser intensity for energies higher than  $19\,100\text{ cm}^{-1}$ .

#### ${}^5D_0$ region

Excitation spectra of the  ${}^7F_0 \rightarrow {}^5D_0$  transition were recorded by scanning the laser from  $17\,100$  to  $17\,500\text{ cm}^{-1}$  and monitoring the emission at different positions inside the  ${}^5D_0 \rightarrow {}^7F_2$  band (see Fig. 9). The absorption profile of the  ${}^7F_0 \rightarrow {}^5D_0$  transition is reproduced for comparison at the top of Fig. 9. Monitoring at a high-energy site ( $16\,490\text{ cm}^{-1}$ ) a relatively narrow (about  $80\text{ cm}^{-1}$  halfwidth) symmetric  ${}^7F_0 \rightarrow {}^5D_0$  excitation spectrum is obtained. The excitation spectra at lower observation energies are redshifted and broadened (about  $94\text{ cm}^{-1}$  for the  $15\,945\text{ cm}^{-1}$  spectrum) with a wing on the high-energy side. This wing can be explained by the coincidence of the energy of two Stark levels of the  ${}^7F_2$  state for two subsets of  $\text{Eu}^{3+}$  ions.

#### Phonon sidebands

Figure 10 shows the phonon sidebands associated with the  ${}^7F_0 \rightarrow {}^5D_0$  excitation transition monitoring at different positions inside the pure electronic emission transition. The wavenumbers on the abscissa are relative to the correspond-

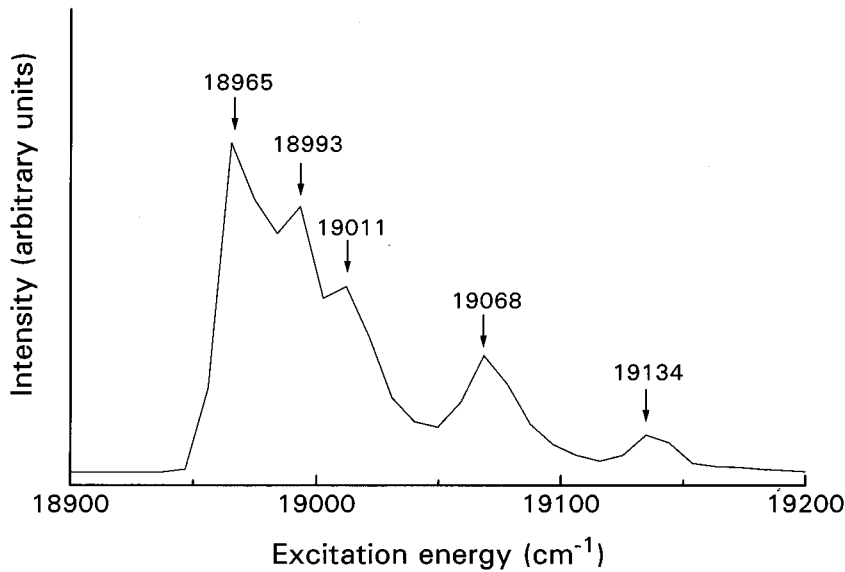


FIG. 7. Excitation spectrum of  $\text{Eu}^{3+}$  in the  $25\text{Na}_2\text{O}\cdot 50\text{B}_2\text{O}_3\cdot 25\text{SiO}_2$  glass in the  ${}^7F_0 \rightarrow {}^5D_1$  region monitored at  $17\,233\text{ cm}^{-1}$  (inside the  ${}^5D_0 \rightarrow {}^7F_0$  band) recorded at 13 K.

ing observation energy, which is indicated at the left side of each trace and serves as a measure for the energy of the sites. All spectra show phonon sidebands in the two regions  $900\text{--}1300\text{ cm}^{-1}$  and  $1300\text{--}1600\text{ cm}^{-1}$  above the zero phonon line (ZPL). Both regions consist of a broad band which is apparently shifted towards smaller energy, when the observation energy is increased. In the low-frequency range Si-O vibrations and, possibly, small contributions of  $\text{BO}_4^-$  vibrations are expected.<sup>34,35</sup> However,  $\text{Eu}^{3+}$  phonon sideband measurements in sodium borate glasses indicate that the  $\text{BO}_4^-$  contribution is small for high sodium contents.<sup>35</sup> In the high-frequency range B-O vibrations from  $\text{BO}_3$  units are located. The asymmetrical bandshapes for  $17\,233\text{ cm}^{-1}$  and higher observation energies, however, suggest that each band consists of at least two vibrational modes. The Si-O peak located at  $1190\text{ cm}^{-1}$  above the  ${}^5D_0 \rightarrow {}^7F_0$  transition of a  $17\,153\text{ cm}^{-1}$  site is shifted to lower energy for higher site energies and is found at  $1150\text{ cm}^{-1}$  for the  $17\,257\text{ cm}^{-1}$  site. Starting with observation energies of  $17\,233\text{ cm}^{-1}$  a second band appears at  $1020\text{ cm}^{-1}$  which remains more or less constant for all higher energy sites.

In the B-O region the peak at  $1550\text{ cm}^{-1}$  of the  $17\,153\text{ cm}^{-1}$  site is also shifted to lower energy as the observation energy is increased. Starting with  $17\,233\text{ cm}^{-1}$  sites it is replaced by a second band centered at  $1380\text{ cm}^{-1}$  which remains at this position for all higher site energies.

#### IV. DISCUSSION

The crystal-field potential  $H_{\text{cf}}$  acting on the  $\text{Eu}^{3+}$  ions is conveniently expressed as

$$H_{\text{cf}} = \sum_{k,q} B_{kq} C_{kq}, \quad (1)$$

where the  $B_{kq}$  are crystal-field parameters and the  $C_{kq}$  are spherical harmonics in Racah normalization.<sup>36,37</sup> We adopt  $C_{2v}$  symmetry for the crystal-field calculations, as this is the highest symmetry for which full splitting of the  ${}^7F_1$  and  ${}^7F_2$  states of  $\text{Eu}^{3+}$  is allowed, and the lowest in which symmetry of most of the components is maintained.<sup>12</sup> Ignoring  $J$  mixing, the three crystal-field energies of the  ${}^7F_1$  multiplet are,<sup>17</sup>

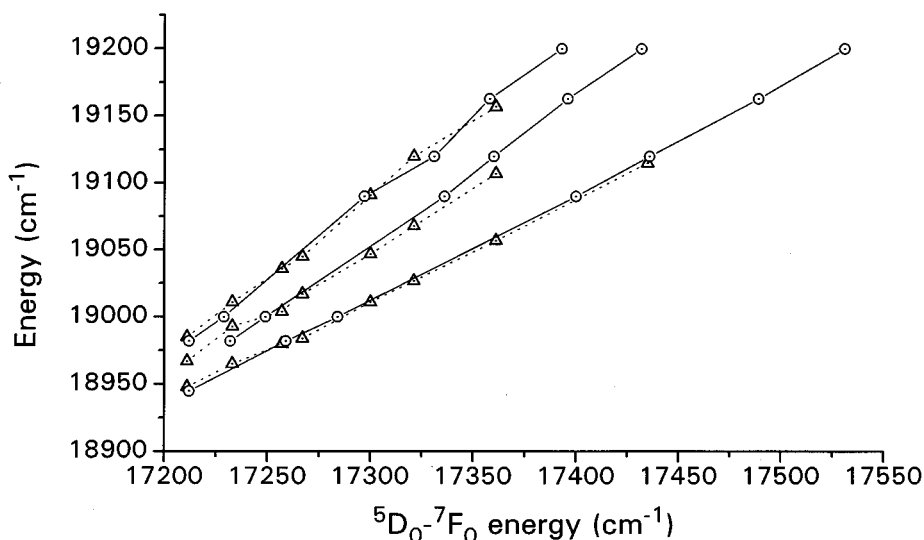


FIG. 8. Comparison of the Stark splitting of the  ${}^5D_1$  state of  $\text{Eu}^{3+}$  in the  $25\text{Na}_2\text{O}\cdot 50\text{B}_2\text{O}_3\cdot 25\text{SiO}_2$  glass at 13 K obtained from FLN spectroscopy (circles) and from site-selective excitation of the  ${}^7F_0 \rightarrow {}^5D_1$  transition (triangles).

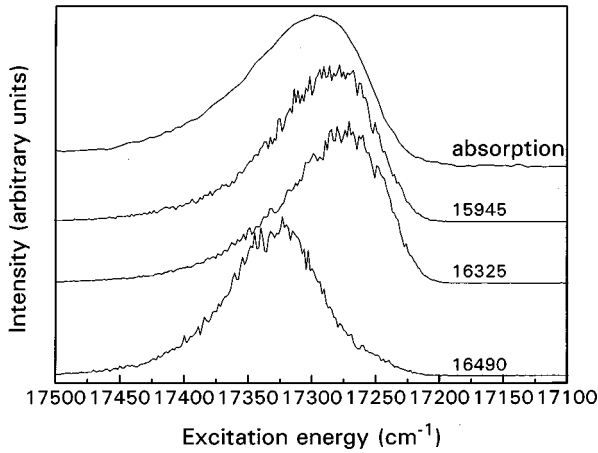


FIG. 9. Excitation spectra of the  ${}^7F_0 \rightarrow {}^5D_0$  transition of  $\text{Eu}^{3+}$  in the  $25\text{Na}_2\text{O} \cdot 50\text{B}_2\text{O}_3 \cdot 25\text{SiO}_2$  glass at 13 K monitored at different positions inside the  ${}^5D_0 \rightarrow {}^7F_2$  emission band. The observation energies are indicated. Top trace: absorption profile of the  ${}^7F_0 \rightarrow {}^5D_0$  transition.

$$E(\varepsilon_0) = E({}^7F_1) + B_{20}/5, \quad (2)$$

$$E(\varepsilon_{\pm}) = E({}^7F_1) - (B_{20} \pm \sqrt{6}B_{22})/10.$$

$E({}^7F_1)$  denotes the barycenter of the  ${}^7F_1$  multiplet and  $\varepsilon_0$ ,  $\varepsilon_+$ , and  $\varepsilon_-$  denote the crystal-field states. Once an assignment of the observed energy levels to these states is established, values for the crystal-field parameters  $B_{20}$  and  $B_{22}$  may be calculated from Eq. (2) for each excitation wavelength. It is generally agreed that, in the FLN spectra, the highest energy feature, which is most sensitive to the excitation energy and usually sharper than the two others, is a transition from  ${}^5D_0$  to the  ${}^7F_1(\varepsilon_0)$  component of the  ${}^7F_1$  state. We assign the three Stark levels as the sequence  $\varepsilon_0$ ,  $\varepsilon_-$ , and  $\varepsilon_+$  with increasing energy. This ordering is consistent with that of Brecher and Riseberg<sup>12</sup> (who use the irreducible representations of  $C_{2v}$  to label the Stark components), and with that of Nishimura and Kushida,<sup>17</sup> but differs from the assignment of Hegarty, Yen, and Weber,<sup>14</sup> who put  $\varepsilon_-$  to lowest energy. For the present investigation an additional assignment to the two major types of sites (I,II) has to be made in order to account for the six rather than three bands in this spectral range.

In oxide glasses the first coordination shell of rare-earth ions consists of oxygens either in the form of nonbridging oxygens carrying a full negative charge or of bridging oxygens carrying a partial negative charge. For electrostatic reasons nonbridging oxygens will be the preferred partners.<sup>37</sup> This species is also more easily drawn towards the  $\text{Eu}^{3+}$  ions because it is connected to the glass network only on one end. Given the borosilicate nature of our glass sample it is reasonable to propose that one of the two major site distributions is related to  $\text{Eu}^{3+}$  ions in an environment of oxygen atoms connected to silicon atoms and the other site distribution to oxygen atoms connected to boron atoms. This behavior was also inferred from the optical spectra of  $\text{Mn}^{2+}$ -doped sodium borosilicate glasses.<sup>38</sup>

The first coordination shell of rare-earth ions in binary alkali silicate glasses is known to be remarkably constant.

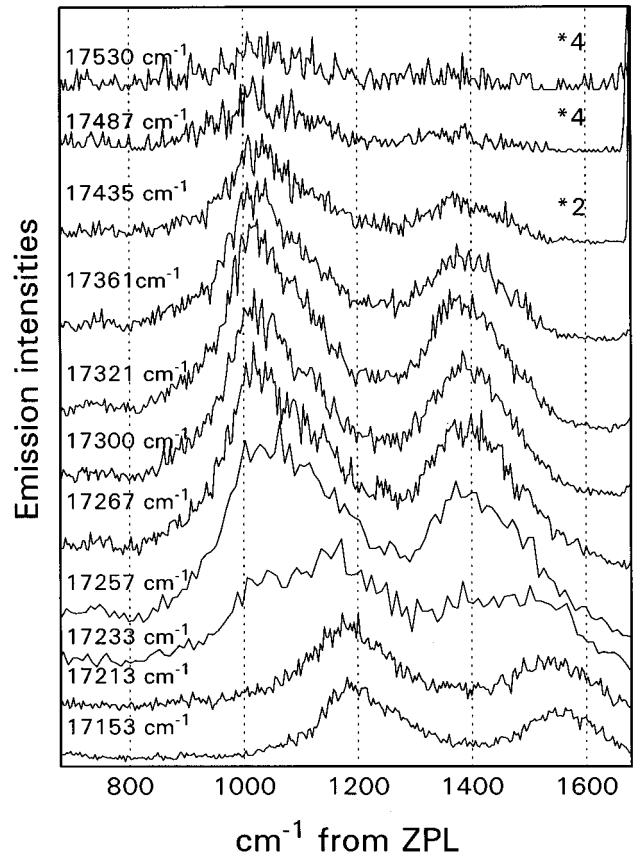


FIG. 10. Excitation spectra of the phonon sideband structure above the  ${}^7F_0 \rightarrow {}^5D_0$  transition of  $\text{Eu}^{3+}$  in the  $25\text{Na}_2\text{O} \cdot 50\text{B}_2\text{O}_3 \cdot 25\text{SiO}_2$  glass recorded at 13 K as a function of the observation energy (vertical displacement) inside the pure electronic transition.

Not only do  $\text{Eu}^{3+}$  ions in sodium silicate glasses with different modifier contents have their  ${}^7F_1$ ,  ${}^5D_0$ , etc. states at exactly the same energy, but Todoroki, Hirao, and Soga<sup>39</sup> have shown that the splitting of the  ${}^7F_1$  state in sodium silicate glasses obtained in FLN experiments as a function of the excitation energy is also independent of the network modifier concentration. Hence the insensitivity of the sites towards compositional changes is given not only for an average over all sites but also for each subset of sites excited by the same energy. If such silicate sites are occupied by  $\text{Eu}^{3+}$  ions in any silicate glass they can easily be identified by their characteristic  ${}^7F_1$  splitting which can be expressed in terms of the two crystal-field parameters  $B_{20}$  and  $B_{22}$ .

In order to make quantitative comparisons with the literature the definition of an average crystal-field parameter  $B_2$ ,<sup>21</sup>

$$B_2 = \sqrt{(B_{20})^2 + 2(B_{22})^2} \quad (3)$$

was adopted.

(Note: Care must be taken when crystal-field parameters from different sources are compared because depending on the explicit form of the crystal-field potential they may have different significance even when they are labeled by the same symbols. In order to make a comparison with the  $B_{kq}$  values of Brecher and Riseberg,<sup>12</sup> we multiplied our  $B_{kq}$  values by a factor of 2 for  $B_{20}$  and  $\sqrt{6/3}$  for  $B_{22}$ , respectively<sup>40</sup>.)

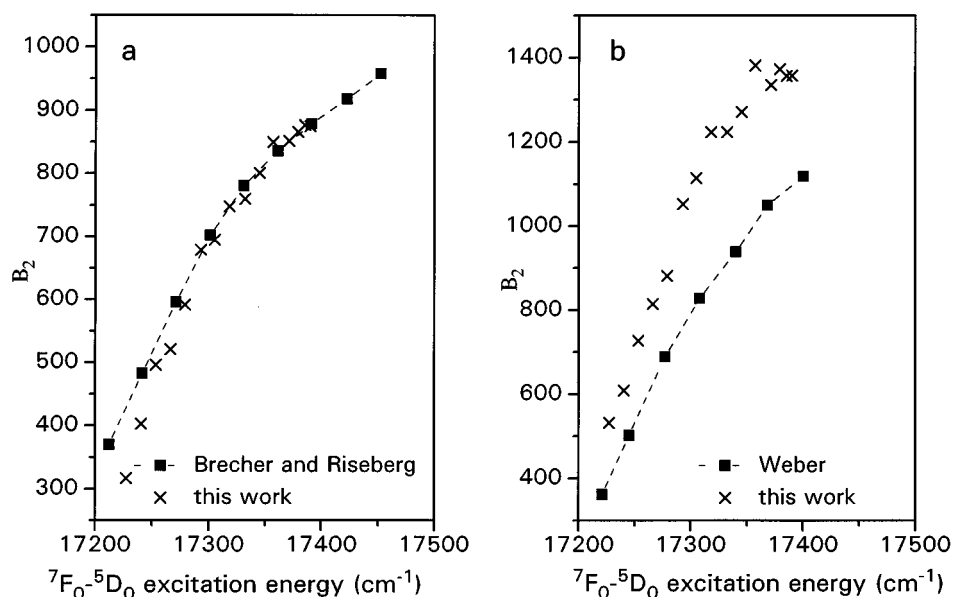


FIG. 11. Comparison of the  $B_2$  values obtained from the  ${}^7F_1$  splitting of  $\text{Eu}^{3+}$  in the  $25\text{Na}_2\text{O}\cdot 50\text{B}_2\text{O}_3\cdot 25\text{SiO}_2$  glass with the corresponding values of (a)  $\text{Eu}^{3+}$  in sodium barium zinc silicate glass (Ref. 12) and (b)  $\text{Eu}^{3+}$  in lithium borate glass (Ref. 22).

We have calculated the  $B_2$  values for all possible combinations of three out of the six observed  ${}^7F_1$  Stark energies of our sample and compared the result with  $B_2$  values for sodium barium zinc silicate<sup>12</sup> [see Fig. 11(a)]. The only combination which leads to  $B_2$  values comparable with the  $B_2$  of the silicate glass is labeled in Fig. 5 as site I and the corresponding  $B_2$  values are shown in Fig. 11(a). The agreement of the two data sets is evident; in fact, the two curves converge for excitation energies higher than  $17\,300\text{ cm}^{-1}$ . The deviation occurs for lower excitation energies where the six Stark components are very close and strongly overlapping each other, such that the curve fits are less reliable.

The remaining three Stark components are consequently labeled as site II and attributed to  $\text{Eu}^{3+}$  in a borate environment. Since the  ${}^7F_1(\epsilon_0)$  energies for both sites are very similar, the value of  $B_2$  is almost independent on the choice of this crystal-field level. The assignment of the lowest Stark level to site I is motivated by the results of the Voigt profile fits (see Fig. 4). Invariably the three bands assigned to site I show a narrower width compared with the bands assigned as site II. Within each site distribution the widths of the  ${}^5D_0 \rightarrow {}^7F_1(\epsilon_-, \epsilon_+)$  transitions are larger than the width of the  ${}^5D_0 \rightarrow {}^7F_1(\epsilon_0)$  transition by a factor of 2. In view of the similarity of  $\text{Eu}^{3+}$  environments in silicate glasses the increase of the  ${}^7F_1$  splitting as a function of the excitation energy is likely to reflect a decrease of the Eu-O distances, inducing an increase in the crystal-field strength, when the energy of the sites increases, rather than dramatic changes of geometry and coordination numbers. The first coordination shell is therefore no longer completely random, which leads to a much narrower site distribution and hence to smaller residual inhomogeneous widths for the observed transitions in the FLN spectra. This description is consistent with the idea of  $\text{Eu}^{3+}$  ions forming quasimolecular complexes<sup>41,42</sup> in the glass rather than occupying random holes in the glass structure.

A further confirmation of this view comes from the  $1020\text{ cm}^{-1}$  band in the phonon sideband structure. We assign it in agreement with Nelson, Furukawa, and White,<sup>41</sup> who found a vibration at  $1024\text{ cm}^{-1}$  by difference Raman spectroscopy on

$\text{Sc}^{3+}$ -doped sodium silicate glasses, which they attributed to Si-O stretching vibrations of  $\text{SiO}_4$  units associated to  $\text{Sc}^{3+}$  ions forming a quasimolecular complex. We assign the second band in the Si-O region at  $1150\text{ cm}^{-1}$  which is dominant in low-energy sites and disappears at higher site energies to Si-O stretching vibrations of  $\text{SiO}_4$  tetrahedra with four bridging oxygens in the  $\text{Eu}^{3+}$  neighborhood. This is consistent with the small crystal-field splitting observed for the low-energy sites.

The situation is much more complicated in sodium borate glasses. For low alkali concentrations (up to  $R=0.40$ ) the appearance of additional lines in the  ${}^5D_0 \rightarrow {}^7F_1$  region points at two major site distributions for  $\text{Eu}^{3+}$  in these binary glasses.<sup>22</sup> This is consistent with the tendency of these glasses towards phase separation. For higher modifier contents a single site distribution is prevalent. The present glass sample with a  $\text{Na}_2\text{O}/\text{B}_2\text{O}_3$  ratio of  $R=0.5$  will certainly belong to the second category. Generally, the splitting of the  ${}^7F_1$  state in borates is found to be slightly larger than in silicates and shows a greater variety depending on the composition.<sup>43</sup> To our knowledge, no crystal-field parameters on  $\text{Eu}^{3+}$ -doped sodium borate glasses have been reported in the literature. In Fig. 11(b) the observed  $B_2$  values for site II of our sample are compared with  $B_2$  values calculated from the crystal-field splitting of the  ${}^7F_1$  state of  $\text{Eu}^{3+}$  in  $40\text{Li}_2\text{O}\cdot 60\text{B}_2\text{O}_3$  glass ( $R=0.66$ ) shown in Fig. 8 of Ref. 22. The agreement is not nearly as good as for the silicate sites; however, considering the different  $R$  values of the two glasses and the fact that in the borate glass a different modifier ( $\text{Li}_2\text{O}$ ) is present, the agreement is reasonable, indicating that our assignment of site II to a borate environment of  $\text{Eu}^{3+}$  is essentially correct. The larger width of the Stark components of site II is consistent with the larger variety of oxygen species in borate glasses (bridging and nonbridging oxygens in planar  $\text{BO}_3$  units, bridging and nonbridging oxygens in tetrahedral  $\text{BO}_4^-$  units). We assign the phonon sideband at  $1550\text{ cm}^{-1}$  to B-O<sup>-</sup> vibrations of weakly coupled  $\text{BO}_3$  units in the neighborhood of  $\text{Eu}^{3+}$ , while the stronger band at  $1380\text{ cm}^{-1}$  which dominates at higher site energies is due to B-O<sup>-</sup> vibrations strongly coupled to  $\text{Eu}^{3+}$ .<sup>44</sup> The in-

crease of the  ${}^7F_1$  splitting with increasing site energy is consistent with the increasing flexibility of glass networks consisting of planar  $\text{BO}_3$  units, because they allow for smaller Eu-O distances in these sites and therefore produce higher crystal-field strengths.

The B-O and Si-O phonon sidebands dominating the spectra at high observation energies can also be seen starting from the observation energy of  $17\,233\text{ cm}^{-1}$ ; they are due to the accidental coincidence already observed in the  ${}^5D_1$  excitation spectra. This coincidence blurs the shift of the vibronic sidebands with the increasing observation energy. Moreover, the phonon sideband due to the Eu-O stretching, which should fall in the region between  $250$  and  $450\text{ cm}^{-1}$ ,<sup>45,48</sup> appears to be unimportant. In fact, in the excitation spectra a very weak and broad feature is barely detectable in this region. The calculated crystal-field parameters for the final assignment of the two sites and the corresponding average crystal-field parameters are given in Table II as a function of the excitation energy.

The splitting of the  ${}^5D_1$  state obtained either by emission after  ${}^5D_1$  excitation or by excitation spectroscopy in the  ${}^7F_0 \rightarrow {}^5D_1$  region also increases in a monotonic way with the excitation energy (see Fig. 5). The ratio of the Stark splittings of the  ${}^5D_1$  to those of  ${}^7F_1$  yields a reduction factor of about 0.18, which is smaller than the value of 0.298 predicted for pure Russell-Saunders states<sup>46</sup> but in good agreement with the experimentally found reduction factor of about 0.2 for crystals and glasses.<sup>14</sup>

## V. CONCLUSIONS

The optical measurements of the phonon sidebands and of the  ${}^7F_1$  Stark splitting give evidence of two different distributions of sites for the  $\text{Eu}^{3+}$  ions, related to the silicate and the borate portions of the glass network. This conclusion is confirmed by the parameters obtained from a crystal-field analysis of the  ${}^7F_1$  splitting. The existence of the two phases in borosilicate glasses is confirmed using  $\text{Eu}^{3+}$  as a probe and the present results agree with the conclusions drawn from NMR and Raman measurements. The fact that  $\text{Eu}^{3+}$  is found in the silicate phase is a strong indication for the presence of sodium ions in the silicate portion of the glass, in agreement with the modified random network theory for the structure of oxide glasses.<sup>47</sup> At the impurity concentration levels considered in the present study, no energy transfer between different sites occurs from the  ${}^5D_0$  and  ${}^5D_1$  states. The intensity of the phonon sidebands is concentrated in the high-frequency stretching modes of the network formers, at variance with what is found for zinc borate glasses in which

TABLE II. Positions of the Stark components  $\varepsilon_0$ ,  $\varepsilon_-$ , and  $\varepsilon_+$  of the  ${}^7F_1$  state of  $\text{Eu}^{3+}$  in  $25\text{Na}_2\text{O}\cdot 50\text{B}_2\text{O}_3\cdot 25\text{SiO}_2$  glass as a function of the excitation energy together with the crystal-field parameters  $B_{20}$  and  $B_{22}$  and the average crystal-field parameter  $B_2$  (a) for site I and (b) for site II. All values are  $\text{cm}^{-1}$ .

Excitation	(a)					
	$\varepsilon_0$	$\varepsilon_-$	$\varepsilon_+$	$B_{20}$	$B_{22}$	$B_2$
17 227	261	388	441	-256	133	317
17 240	247	401	472	-316	178	403
17 253	236	395	495	-348	250	496
17 266	220	402	501	-386	248	521
17 279	206	414	526	-440	280	592
17 293	191	426	556	-500	325	679
17 305	181	436	563	-531	318	695
17 318	170	441	579	-567	345	748
17 332	162	456	588	-600	330	760
17 345	155	465	604	-633	348	801
17 357	147	477	624	-673	368	850
17 371	139	489	627	-698	345	852
17 379	137	499	636	-718	343	866
17 385	133	503	640	-731	343	877
17 390	130	506	639	-738	333	875
Excitation	(b)					
	$\varepsilon_0$	$\varepsilon_-$	$\varepsilon_+$	$B_{20}$	$B_{22}$	$B_2$
17 227	290	354	491	-221	343	532
17 240	272	354	509	-266	388	609
17 253	271	339	530	-273	478	728
17 266	251	337	549	-320	530	815
17 279	236	352	577	-381	563	882
17 293	218	334	607	-421	683	1053
17 305	204	338	625	-463	718	1115
17 318	198	334	651	-491	793	1224
17 332	188	345	658	-523	783	1224
17 345	183	357	680	-559	808	1272
17 357	173	367	717	-615	875	1382
17 371	166	387	718	-644	828	1336
17 379	160	392	731	-669	848	1373
17 385	154	397	729	-682	830	1357
17 390	151	399	730	-689	828	1358

the Eu-O mode is dominant.<sup>48,49</sup>

## ACKNOWLEDGMENT

The authors gratefully thank Dr. A. Speghini, University of Verona, for helpful discussions.

<sup>1</sup>P. Taylor, S. D. De Vaal, and D. G. Owen, *Am. Ceram. Soc. Bull.* **65**, 1513 (1986).

<sup>2</sup>D. Rai, A. R. Felmy, R. W. Fulton, and J. L. Ryan, *Radiochim. Acta* **58/59**, 9 (1992).

<sup>3</sup>Y. H. Yun and P. J. Bray, *J. Non-Cryst. Solids* **27**, 363 (1978).

<sup>4</sup>S. Z. Xiao, *J. Non-Cryst. Solids* **45**, 29 (1981).

<sup>5</sup>W. J. Dell, P. J. Bray, and S. Z. Xiao, *J. Non-Cryst. Solids* **58**, 1 (1983).

<sup>6</sup>W. L. Konijnendijk and J. M. Stevels, *J. Non-Cryst. Solids* **20**, 193 (1976).

<sup>7</sup>B. C. Bunker, D. R. Tallant, R. J. Kirkpatrick, and G. L. Turner, *Phys. Chem. Glasses* **31**, 30 (1990).

<sup>8</sup>K. Gatterer, G. Pucker, and H. P. Fritzer (unpublished).

<sup>9</sup>M. J. Weber, J. A. Paisner, S. S. Sussman, W. M. Yen, L. A. Riseberg, and C. Brecher, *J. Lumin.* **12/13**, 729 (1976).

<sup>10</sup>M. J. Weber, in *Laser Spectroscopy of Solids*, edited by W. M.

- Yen and P. M. Selzer (Springer-Verlag, Berlin, 1981), p. 189.
- <sup>11</sup>G. F. Imbusch, Phys. Scr. T **19**, 354 (1987).
- <sup>12</sup>C. Brecher and L. A. Riseberg, Phys. Rev. B **13**, 81 (1976).
- <sup>13</sup>O. K. Alimov, T. T. Basiev, Yu. K. Voron'ko, L. S. Gaigerova, and A. V. Dmitryuk, Sov. Phys. JETP **45**, 690 (1977).
- <sup>14</sup>J. Hegarty, W. M. Yen, and M. J. Weber, Phys. Rev. B **18**, 5816 (1979).
- <sup>15</sup>C. Brecher and L. A. Riseberg, J. Non-Cryst. Solids **40**, 469 (1980).
- <sup>16</sup>Xu Gang, G. Boulon, and R. Powell, J. Chem. Phys. **78**, 4374 (1983).
- <sup>17</sup>G. Nishimura and T. Kushida, Phys. Rev. B **37**, 9075 (1988).
- <sup>18</sup>T. F. Belliveau and D. J. Simkin, J. Non-Cryst. Solids **110**, 127 (1989).
- <sup>19</sup>J. A. Capobianco, P. P. Proulx, M. Bettinelli, and F. Negrisolo, Phys. Rev. B **42**, 5936 (1990).
- <sup>20</sup>G. Cormier, J. A. Capobianco, C. A. Morrison, and A. Monteil, Phys. Rev. B **48**, 16 290 (1993).
- <sup>21</sup>R. Balda, J. Fernandez, H. Eilers, and W. M. Yen, J. Lumin. **59**, 81 (1994).
- <sup>22</sup>M. J. Weber, J. Hegarty, and D. H. Blackburn, in *Borate Glasses*, edited by L. D. Pye, V. D. Frechette, and N. J. Kreidl (Plenum, New York, 1978), p. 215.
- <sup>23</sup>F. Durville, G. Boulon, R. Reisfeld, H. Mack, and C. K. Jørgensen, Chem. Phys. Lett. **102**, 393 (1983).
- <sup>24</sup>J. A. Capobianco, T. F. Belliveau, G. Lord, D. J. Simkin, J. Tait, and P. J. Hayward, Phys. Rev. B **34**, 4204 (1986).
- <sup>25</sup>J. L. Adam, V. Poncon, J. Lucas, and G. Boulon, J. Non-Cryst. Solids **91**, 191 (1987).
- <sup>26</sup>J. Dexpert-Ghys, B. Piriou, N. Jacquet-Francillon, and C. Sombret, J. Non-Cryst. Solids **125**, 117 (1990).
- <sup>27</sup>J. A. Capobianco, P. P. Proulx, B. Andrianasolo, and B. Champagnon, Phys. Rev. B **43**, 10 031 (1991).
- <sup>28</sup>S. Todoroki, K. Hirao, and N. Soga, J. Appl. Phys. **72**, 5853 (1992).
- <sup>29</sup>N. B. Brachkovskaya, S. G. Lunter, A. K. Przhevuskii, E. L. Raaben, and M. N. Tolstoi, Opt. Spectrosc. (USSR) **43**, 411 (1977).
- <sup>30</sup>F. Fermi, L. Tellini, G. Ingletto, A. Vinanttieri, and M. Bettinelli, Inorg. Chim. Acta **150**, 141 (1988).
- <sup>31</sup>Y. Nageno, H. Takebe, K. Morinaga, and T. Izumitani, J. Non-Cryst. Solids **169**, 288 (1994).
- <sup>32</sup>R. Reisfeld, Struct. Bonding (Berlin) **22**, 123 (1975).
- <sup>33</sup>E. W. J. L. Oomen and A. M. A. van Dongen, J. Non-Cryst. Solids **111**, 205 (1989).
- <sup>34</sup>S. Todoroki, S. Tanabe, K. Hirao, and N. Soga, J. Non-Cryst. Solids **136**, 213 (1991).
- <sup>35</sup>S. Tanabe, S. Todoroki, K. Hirao, and N. Soga, J. Non-Cryst. Solids **122**, 59 (1990).
- <sup>36</sup>B. G. Wybourne, *Spectroscopic Properties of Rare Earths* (Wiley-Interscience, New York, 1956).
- <sup>37</sup>K. Gatterer, G. Pucker, H. P. Fritzer, and S. Arafa, J. Non-Cryst. Solids **176**, 237 (1994).
- <sup>38</sup>P. E. Menassa, D. J. Simkin, and P. Taylor, J. Lumin. **35**, 223 (1986).
- <sup>39</sup>S. Todoroki, K. Hirao, and N. Soga, J. Appl. Phys. **72**, 5853 (1992).
- <sup>40</sup>A. J. Kassman, J. Chem. Phys. **53**, 4118 (1970).
- <sup>41</sup>C. Nelson, T. Furukawa, and W. B. White, Mater. Res. Bull. **18**, 959 (1983).
- <sup>42</sup>C. Nelson, D. R. Tallant, and J. A. Shelnutt, J. Non-Cryst. Solids **68**, 87 (1984).
- <sup>43</sup>P. K. Gallagher, C. R. Kurkjian, and P. M. Bridenbaugh, Phys. Chem. Glasses **6**, 95 (1965).
- <sup>44</sup>G. Blasse and G. J. Dirksen, Inorg. Chim. Acta **145**, 303 (1988).
- <sup>45</sup>A. Piazza, A. Bouajaj, M. Ferrari, M. Montagna, R. Campostrini, and G. Carturan, J. Phys. (Paris) Colloq. **55**, C4-569 (1994).
- <sup>46</sup>B. R. Judd, Proc. R. Soc. London Ser. A **228**, 120 (1955).
- <sup>47</sup>G. N. Greaves, J. Non-Cryst. Solids **71**, 203 (1985).
- <sup>48</sup>L. Ambrosi, M. Bettinelli, M. Ferrari, M. Casarin, and A. Piazza, J. Phys. (Paris) Colloq. **55**, C4-477 (1994).
- <sup>49</sup>M. Bettinelli, A. Speghini, M. Ferrari, and M. Montagna, J. Non-Cryst. Solids (to be published).